[57]Thomson, W. T., *Vibration Theory and Applications,* Prentice-Hall, Englewood Cliffs, N.J., 1965, pp. 84–86.

[58]Greene, R. B., "Gyroscopic Effects on the Critical Speeds of Flexible Rotors," *ASME Transactions, Journal of Applied Mechanics,* Vol. 70, 1948, pp. 369–376.

[59]Huang, T. C. and Huang, F. C. C., "On Precession and Critical Speeds of Two-Bearing Machines with Overhung Weight," ASME Paper 76-VIBR-19, 1967 ASME Vibrations Conference, Boston, Mass., March 1967. (Also published in the *ASME Transactions,* Ser. B: *Journal of Engineering for Industry,* Vol. 89, Sec. 1, pp. 713–718).

[60]Curwen, P. W., "Feasibility of Gas Bearings for Small High Performance Aircraft Gas Turbines," USAAVLABS Tech. Rept. 68-87, 1968, U.S. Army Aviation Material Labs., Fort Eustis, Va.

[61]Nypan, L. J., Scibbe, H. W., and Hanrock, B. J., "Optimal Speed Sharing Characteristics of a Series-Hybrid Bearing," *ASME Transactions,* Ser. F: *Journal of Lubrication Technology,* Vol. 95, Sec. 4, Jan. 1973, pp. 76–81.

APRIL 1975 J. AIRCRAFT VOL. 12, NO. 4

Dynamic Response of Viscous-Damped Multi-Shaft Jet Engines

David H. Hibner*

Pratt & Whitney Aircraft Division, United Aircraft Corporation, East Hartford, Conn.

Rotor synchronous vibration experienced on multi-shaft aircraft engines results directly from rotor imbalance exciting the numerous critical speeds inherent in light-weight, high-speed modern powerplants. The understanding and reduction of this dynamic response is essential during engine design and development phases. This paper presents an efficient analytical technique capable of predicting the vibratory response of an engine with nonlinear viscous damping. A unique transfer-matrix method is applied to the idealized equivalent engine system to produce an unusually small array of influence coefficients. The damper equations for a closed-end viscous damper are derived from the basic Reynolds equation. The analysis is applied to a two-shaft aircraft engine to illustrate the basic concepts of multi-shaft critical speeds and nonlinear viscous-damped response.

Nomenclature

c = damper radial clearance
e = damper eccentricity
g = gravitational constant
h = damper film thickness
k_t = shear stiffness shape factor
l = length of beam element
m = mass
t = time
u = imbalance
x, y, z = rectangular coordinates
A = area
A_{ij} = influence coefficients
B = damping coefficient
D = damper journal diameter
E = elastic modulus
G = shear modulus
I = area moment of inertia
I_g = $(I_P - I_T)g$
I_P = polar moment of inertia
I_T = transverse moment of inertia
K = stiffness
L = length of damper journal
M, N = beam moment components
M' = moment resulting from imbalance force
P = damper oil film pressure
Q = state variables (shear moment, slope, deflection)
Q' = state variables resulting from imbalance force
R = damper journal radius
S = Sommerfeld number
T = torsional stiffness
T = moment imbalance
U, V = beam shear components
U', V' = beam shear components resulting from imbalance forces
U_y = imbalance in y-plane
U_z = imbalance in z-plane
Y, Z = beam deflection components
α = influence coefficients
β = boundary condition coefficients
ϵ = e/c (damper attitude)
η = phase angle of applied moment imbalance
θ = angle from line of centers, viscous damper
θ, γ = beam slope components
μ = oil viscosity
ν = mass/unit length
ϕ = phase angle of applied force imbalance
ϕ = viscous damper phase angle
ω_1 = inner journal spin speed
ω_2 = outer journal spin speed
ω = spin speed
Ω = whirl speed
$*$ = starred state variables represent values on left of massless beam

Subscripts

n = mass stations
L = line
N = span

Received August 7, 1974.

Index categories: Aircraft Vibration; Structural Dynamic Analysis.

*Project Engineer.

Introduction

THE importance of rotor dynamic technology has increased significantly during the past five years, and today this technology impacts the gas-turbine engine bearing configuration, the development program, certification requirements, and manufacturing and assembly procedures. A definition of the engine critical speeds and steady-state response to inherent rotor imbalance is required to allow the engineer to optimize the rotor and case structure for minimum weight and sensitivity to imbalance. The complex vibration response which results from a multishaft, high-speed, lightweight engine structure must be conveyed to the design engineer in a manner that allows easy manipulation of the design variables in order to produce the best structure with current technology.

The technical literature contains numerous rotating-machinery forced-response analyses which are extensions of the general theory of transfer matrix methods for transverse vibration as originally presented by Myklestad[1] and Prohl.[2] Prohl applied classical beam theory to rotating shafts and calculated the simply supported natural frequencies (critical speeds) considering symmetric, flexi-

ble bearings, and the gyroscopic moments for forward synchronous whirl. Green[3] extended the concept of gyroscopic moments to account for both forward and backward whirl of single- and multiple-disk rotors and Yamamoto[4] presented both analytical and experimental evidence of backward whirl in rotor-bearing systems. Major extensions of the original works of Myklestad and Prohl did not appear in the literature until the early 1960's when Koenig[5] presented a method whereby both natural frequencies and response to imbalance of flexibly mounted rotors could be calculated. The major limitation was the single-plane analysis which prevented a rigorous treatment of bearing damping. Tang and Trumpler[6] extended Koenig's work to allow rotor deflections in a space curve and could thereby properly account for bearing damping in forced-response calculations. This extension, however, required the transfer matrix to be expressed in complex notation. The major significance of the work was the solution of the forced response of the entire rotor span with only a 2 by 2 complex matrix of influence coefficients which related initial slope and deflection of the span to the moment and shear at the final mass station.

Consideration was given to a technique whereby the influence of nonlinear journal bearings could be accounted for by an iterative procedure. Lund[7,8] extended the theory of forced response calculations to account for asymmetric bearing characteristics. The equations presented in Ref. 8 accounted for continuous mass properties of the shaft but it was noted that no appreciable loss of accuracy occurred when a sufficient number of lumped mass stations were considered. The literature concerning rotating-equipment vibration has predominantly treated the problems of single-rotor systems or systems having axial couplings (Lemke[9]). The effects of the case structure or any other rotating member have received very little attention. Sevick[10] presented the analysis of a multiple-connected structure which was solved by the span approach. This method of solution is, in general, very inefficient because of the large matrix which must be manipulated. A paper by Bohm[11] improved upon the solution procedure for multiple-rotor systems but the equations presented did not properly account for general gyroscopic moment present in dual-rotor gas turbine engines. In addition, shear flexibility and nonlinear fluid-film dampers were not considered. Presented herein is an analytical technique which builds on and extends the synchronous vibration response analyses reported in the literature to a level where accurate total response of multi-shaft gas turbine engines with both linear and nonlinear damping can be predicted.

General Description of Analysis

The typical gas turbine engine requires a complex analysis to accurately predict response from rotor imbalance throughout the entire engine power range. This paper considers an engine with two shafts typically denoted as the low rotor and the high rotor. These two rotors consist of compressor and turbine stages which are connected by flexible shafting. They have a minimum of two rolling-contact bearings each of which is mounted to the case structure through bearing-support structures and may incorporate an intershaft bearing to provide support for one rotor from the other. The two rotors are aerodynamically coupled and have a complex low/high speed relationship. In order to achieve a thorough understanding of the analysis of multi-shaft viscous-damped engines a brief discussion of the capabilities, considerations, assumptions, and provisions in the analysis will be presented.

The vibratory amplitude measured on gas-turbine engines is described as either low-rotor frequency or high-rotor frequency. Low-rotor frequency response results from imbalance in the low rotor as engine resonant frequencies are traversed. Similarly, high-rotor frequency response results from imbalance in the high rotor. In order to define the nature of the critical speeds or the peak response speeds, those which are excited by low-rotor imbalance throughout the low-rotor speed range are designated as low-rotor excited (LRX), and those associated with the high-rotor are designated as high-rotor excited (HRX). Since the two rotors each have different speeds at a given power setting, a separate critical-speed analysis and forced response analysis is necessary for the frequency range of each rotor. The speed of the other rotor must be defined to account for its gyroscopic effects. Thus, the dynamic response analysis properly treats the spin and whirl speeds of each rotor and defines the LRX and HRX critical speeds and response to imbalance.

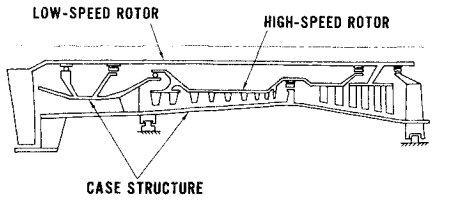

Fig. 1 Two-shaft engine.

The forced-response analysis of a complete two-rotor engine with nonlinear damping requires a unique approach to the typical transfer matrix method for calculating the response along and between the rotor and case structure of an engine. For a system similar to that shown in Fig. 1 a brute-force approach to define the shear, moment, slope, and deflection within each beam could require 120 variables (8 variables/beam). This many simultaneous equations can be handled on a large computer but there is quite often a loss of accuracy. In addition, a considerable amount of computer time is required. The analysis in this paper will present a method which can fully define the response of the engine in Fig. 1 with only 16 simultaneous equations. Thus, matrix manipulation which is necessary in the transfer matrix method is greatly simplified. Simply stated, only two variables, deflection and slope, are needed for each line (the array of axially connected beams) when the transfer matrix is established. In practice, the influence coefficients across the entire line are developed by considering the boundary conditions and compatibility equations at the junction of all beams and at the interconnection of all lines via springs and dampers. By expressing the resulting moment and shear at the right-hand side of each line in terms of unit slopes and deflections at the left end of each line via influence coefficients, the inversion of this matrix of influence coefficients fully defines the deflection and slope of each line in terms of moment and shear at the right-hand ends. For a critical-speed analysis, the search for a speed causing the determinant to go to zero is all that is required. For forced response analysis, the right-hand end moments and shears for applied imbalances are calculated, the deflection and slope on the left-hand side are therefore known, and by standard transfer techniques the mode shape in all variables is fully defined.

Analysis—Method of Solution

The application of the transfer matrix method to fully characterize the vibratory response of a complex gas turbine engine must begin with the calculation of the influence coefficients α_{ij} for each span of the idealized equivalent engine system. Spans are defined as the entire beam between any inter-connecting springs or dampers or any springs or dampers which connect to ground. In the idealized engine diagram (Fig. 2), it is seen that the engine comprises 15 spans distributed through 4 lines. The shear, moment, slope, and deflection within each beam are defined in terms of speed, mass inertia, bending flexibility,

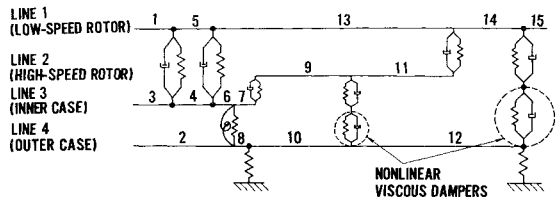

Fig. 2 Two-shaft engine diagram indicating spans and lines.

shear flexibility, length, and load, and are calculated across each mass and massless elastic beam section by a finite difference method which produces 16 influence coefficients. The equations to produce these influence coefficients are derived in Appendix A from the Timoshenko beam equations for a radially symmetric beam element, and fully determine the four state-variables (shear, moment, slope and deflection) at the right end of each span in terms of unit shear, moment, slope, and deflection applied on the left end [Eq. (1)]. The coefficients are calculated for each span.

$$Q_{i_{\text{RIGHT}}} = \alpha_{ij} Q_{j_{\text{LEFT}}} \tag{1}$$

In addition to the span influence coefficients, the boundary conditions and the compatibility equations at the ends and junctions of all spans must be defined in terms of the state-variables and the spring and damping constants. For each span, Eq. (2) is required to define the boundary conditions and compatibility.

$$Q_{i_{\text{LEFT}}} = \beta_{ij} Q_{j_{\text{RIGHT}}} \tag{2}$$

A compact set of equations can be obtained if the state-variables can be defined across the entire line. By accomplishing this in terms of only two variables (slope and deflection) on the left ends of each line to define the moment and shear on the right end of each line, a relatively small matrix can be written to produce a) the characteristic determinant required for critical speed and b) the non-homogeneous equations required for forced response. To perform this feat, an intermediary matrix of coefficients α_{ij}' is calculated from the influence coefficients α_{ij} and the boundary condition coefficients β_{ij}. The matrix α_{ij}' defines the state-variables at the left end of each span in terms of unit slopes and deflections applied on the left ends of each line [Eq. (3)]. The matrix is obtained by a systematic calculation which prevents unknowns, which result at the span junctions, from occurring in the equations; i.e., all lines must be systematically traversed so that when the variables at the left end of each span are defined they are defined only in terms of line left end slopes and deflections.

$$\begin{bmatrix} Q_1 \\ \cdot \\ \cdot \\ \cdot \\ Q_N \end{bmatrix}_{\substack{\text{SPAN} \\ \text{LEFT}}} = \begin{bmatrix} \alpha_{ij}' \end{bmatrix} \begin{bmatrix} \theta_1 \\ Y_1 \\ \vdots \\ \theta_L \\ Y_L \end{bmatrix}_{\substack{\text{LINE} \\ \text{LEFT}}} \tag{3}$$

To complete the influence coefficient definition across the entire line, the last span of each line and the line right-hand boundary conditions together with specific α_{ij}' produce influence coefficients α_{ij}'' which define the line right variables in terms of the line left-end slopes and deflections [Eq. (4)].

$$\begin{bmatrix} Q_1 \\ \cdot \\ \cdot \\ \cdot \\ Q_L \end{bmatrix}_{\substack{\text{LINE} \\ \text{RIGHT}}} = \begin{bmatrix} \alpha_{ij}'' \end{bmatrix} \begin{bmatrix} \theta_1 \\ Y_1 \\ \vdots \\ \theta_L \\ Y_L \end{bmatrix}_{\substack{\text{LINE} \\ \text{LEFT}}} \tag{4}$$

Since the slope and deflection on the right end can be defined in terms of the moment and shear, only these variables are retained and the resulting equations reduce to Eq. (5).

$$\begin{bmatrix} M_1 \\ U_1 \\ \vdots \\ M_L \\ U_L \end{bmatrix}_{\substack{\text{LINE} \\ \text{RIGHT}}} = \begin{bmatrix} A_{ij} \end{bmatrix} \begin{bmatrix} \theta_1 \\ Y_1 \\ \vdots \\ \theta_L \\ Y_L \end{bmatrix}_{\substack{\text{LINE} \\ \text{LEFT}}} \tag{5}$$

This matrix A_{ij} fully defines the characteristics of the entire engine in terms of speed. The matrix size is only two times the number of lines for a critical speed analysis and twice that size for a damped forced-response analysis.

Since the moment and shear at the line right end must be zero to satisfy the boundary conditions, iteration on speed to determine $|A_{ij}| = 0$ produces the natural frequencies of the engine. Assuming unit displacement or slope on a line left end provides a set of determinate equations which through back substitution define the slope and deflection of all line left ends. A complete, but systematic, pass through the spans using the influence coefficients and the boundary coefficients and compatibility equations produces the four state variables and thus the mode shape.

To calculate the response due to rotating imbalance, the influence coefficients α_{ij} are obtained as shown above but the boundary conditions and compatibility equations are calculated considering linear damping elements at span ends where required. The α_{ij}' matrix is calculated for two perpendicular planes [Eq. (6)]. Additional terms due to specific moment and shear imbalance are calculated by applying zero initial conditions on the left ends of all lines. The α_{ij}'' matrix is built as before and the final series of equations are shown in Eq. (7).

$$\begin{bmatrix} Q_1 \\ \cdot \\ \cdot \\ \cdot \\ Q_N \end{bmatrix}_{\substack{\text{SPAN} \\ \text{LEFT}}} = \begin{bmatrix} \alpha_{ij}' \end{bmatrix} \begin{bmatrix} \theta_1 \\ Y_1 \\ \vdots \\ \theta_L \\ Y_L \end{bmatrix}_{\substack{\text{LINE} \\ \text{LEFT}}} + \begin{bmatrix} Q'_1 \\ \cdot \\ \cdot \\ \cdot \\ Q'_N \end{bmatrix} \tag{6}$$

$$\begin{bmatrix} M_1 \\ U_1 \\ \vdots \\ M_L \\ U_L \end{bmatrix}_{\substack{\text{LINE} \\ \text{RIGHT}}} = \begin{bmatrix} A_{ij} \end{bmatrix} \begin{bmatrix} \theta_1 \\ Y_1 \\ \vdots \\ \theta_L \\ Y_L \end{bmatrix}_{\substack{\text{LINE} \\ \text{LEFT}}} + \begin{bmatrix} M'_1 \\ U'_1 \\ \vdots \\ M'_L \\ U'_L \end{bmatrix} \tag{7}$$

To satisfy the boundary conditions, the moment and shear at the line right ends must be zero. Since moments and shears due to imbalance are known, the slopes and deflections on the line left ends to satisfy the boundary conditions are calculated as shown in Eq. (8).

$$\begin{bmatrix} A_{ij} \end{bmatrix} \begin{bmatrix} \theta \\ Y \end{bmatrix} + \begin{bmatrix} M \\ U \end{bmatrix} = 0$$

$$\begin{bmatrix} A_{ij} \end{bmatrix}^{-1} \begin{bmatrix} A_{ij} \end{bmatrix} \begin{bmatrix} \theta \\ Y \end{bmatrix} + \begin{bmatrix} A_{ij} \end{bmatrix}^{-1} \begin{bmatrix} M \\ U \end{bmatrix} = 0 \tag{8}$$

$$\begin{bmatrix} \theta \\ Y \end{bmatrix} = - \begin{bmatrix} A_{ij} \end{bmatrix}^{-1} \begin{bmatrix} M \\ U \end{bmatrix}$$

A complete but systematic pass through the spans and the α_{ij}' equations produces a complete forced-response mode shape in the variables, shear, moment, slope, and deflection in two perpendicular planes. Specific span, spring, and damper energies are calculated as shown in Appendix C.

The response of an engine with nonlinear viscous dampers (a fluid-filled annulus surrounding a bearing as shown in Fig. 3) is obtained with the above linear, damped forced

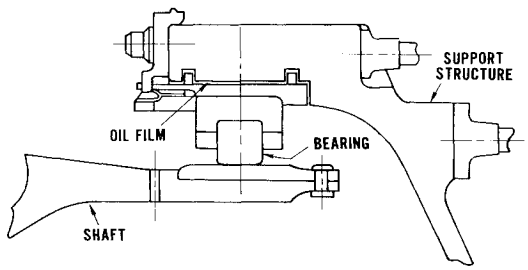

Fig. 3 Nonlinear viscous damper cross section.

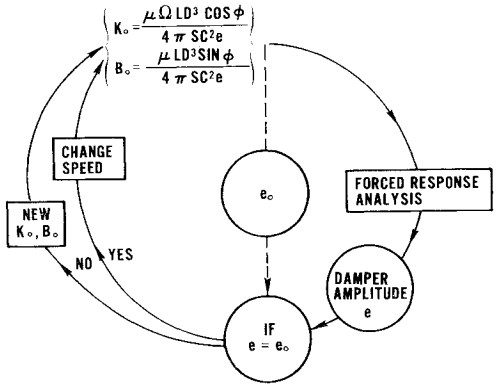

Fig. 4 Forced response analysis iteration scheme for nonlinear viscous damper.

response analysis by simultaneously satisfying the hydrodynamic damper equations derived in Appendix D.

$$K = \frac{\mu\Omega LD^3 \cos\phi}{4\pi SC^2 e} \qquad (9)$$

$$B = \frac{\mu LD^3 \sin\phi}{4\pi SC^2 e}$$

Equation (9) provides the total load generated by a whirling shaft in terms of two variables, K and B, in line with and perpendicular to the shaft deflection. These variables are nonlinearly dependent upon the damper eccentricity (e) since the Sommerfeld number S and phase angle ϕ are also functions of eccentricity.[12] To obtain the response of a viscous-damped engine, an iterative procedure is required at each speed where values of stiffness and damping produce a specific eccentricity at the damper location that must simultaneously satisfy Eq. (9) (see Fig. 4). A solution at all speeds provides the nonlinear viscous-damped response via a linear analysis.

Application of the Analysis

Insight into the natural frequencies of a multi-shaft jet engine with high-inertia discs (fan and turbine wheels) can be obtained by applying the analysis to a two-shaft rig with inter-connected flexible rotors and flexible supports to ground as shown in Fig. 5. The speed ranges of the low and high rotors are, respectively, 4000 and 8000 rpm. An analysis of the system has been performed to obtain all natural frequencies of the shafts both co-rotating and counter-rotating within their speed ranges. Figure 6 displays the forward and backward high-rotor excited natural frequencies for any speed of the low rotor within its limits in a manner similar to the Yamamoto[4] frequency plot. The ordinate for Fig. 6 is the spin and whirl speed for the exciting rotor; the positive coordinate being forward or positive whirl with respect to spin while the negative coordinate denotes backward or negative whirl with respect to the spin direction. The abscissa is the spin speed of the other rotor. The four quadrants of this "map" represent four distinct sets of natural frequencies; all either forward or backward synchronous with respect to the exciting rotor. The upper-right quadrant is the most common set for the two-spool gas turbine engine and is labeled forward synchronous corotating. These natural frequencies are rotor-imbalance-excited critical speeds and are determined for a specific low/high rotor speed relationship line, a–a′. A shift in this speed relationship can drastically change the critical speeds as is shown by line b–b′ in Fig. 6; critical speeds and associated mode shapes of these two speed relationships are shown in Fig. 7. The upper-left quadrant is also labeled forward synchronous, but is for a counter-rotating shaft system. This set of natural frequencies is considerably different than the co-rotating set because of the gyroscopic inertia effects which result from the other rotor spinning in a direction opposite to the whirl speed. The lower quadrants represent backward synchronous co-rotating and counter-rotating natural frequencies which are normally excited by nonlinearities in the system.

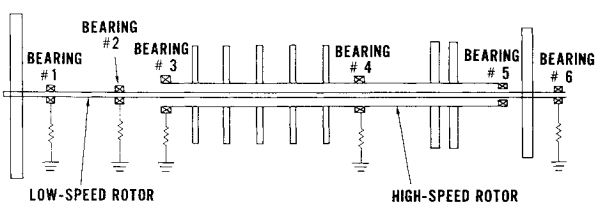

Fig. 5 Two-shaft rig schematic.

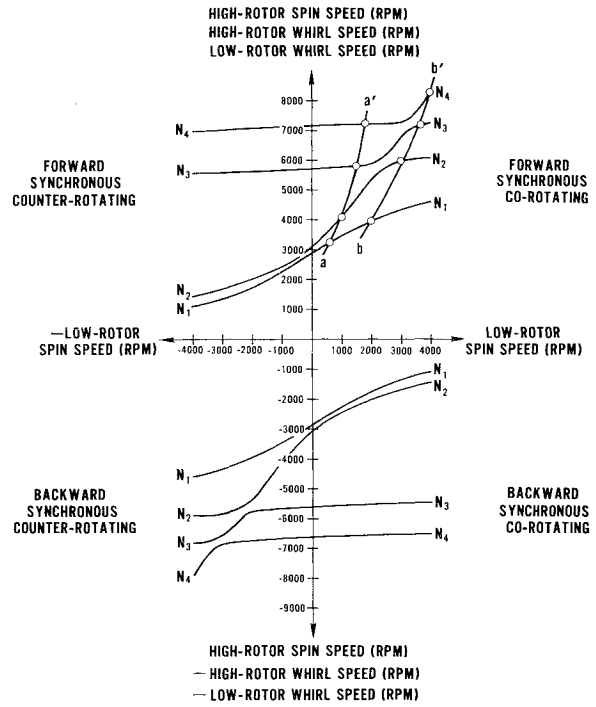

Fig. 6 Natural-frequency map for two-shaft rig.

Construction of the LRX and HRX natural-frequency maps requires a large number of calculations but they provide a great deal of insight into the dynamical system. For the rig system shown, the HRX natural frequencies are dramatically affected by the spin speed of the low rotor. This is quite common since the largest (and highest inertia) disks are usually on the low rotor. The calculation of the information required for the complete map is usually not done, nor is it necessary since an equation representing the speed of one rotor with respect to the other can be included in the analysis directly. Specifically, during the calculation of the influence coefficients the actual spin (ω) and whirl (Ω) speeds are incorporated directly into the terms containing inertia; for example, in the moment equation

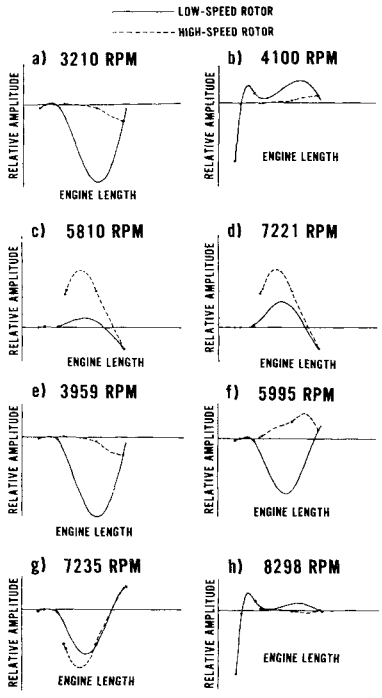

Fig. 7 Two-shaft rig critical-speed mode shapes; figs. a–d represent mode shapes on speed line a–a' in Fig. 6; figs. e–h represent mode shapes on speed line b–b'.

$$M = \ldots + \left(\frac{2\omega}{\Omega} - 1\right)\Omega^2 I\theta + \ldots \qquad (10)$$

Thus, the low-rotor-excited and high-rotor-excited gas turbine engine critical speeds are calculated directly by specifying the rotor speed relationships.

Understanding of the forced-response analysis can be obtained by analyzing a two-shaft gas-turbine engine (Fig. 1) usually described as four inter-connected beams (lines) which represent two shafts and two cases (Fig. 2). The engine being analyzed has two viscous dampers, one on each shaft, and includes linear damping at other locations. Bearing, bearing support, and mount springrates are included in the analysis as well as the bending and shear stiffnesses of both shafts and cases. The total system consists of 312 masses, each with an associated polar moment of inertia. The rotor-speed relationships are included to provide the low and high rotor synchronous response to rotating imbalance. A number of imbalances are included on each rotor to approximate the largest imbalance expected in a large quantity of production engines. Typical amplitude response vs speed is shown in Fig. 8 for a point on the outer case. Both the low and high rotor excited response amplitudes are shown for the engine with and without the viscous dampers. A significant reduction for

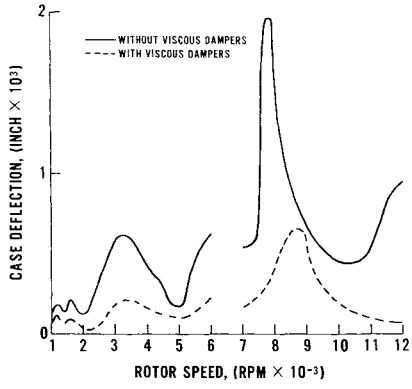

Fig. 8 Calculated response of two-shaft engine.

Table 1 Energy distribution

	Kinetic energy (in.-lb)	Strain energy (in.-lb)	Energy dissipated per cycle (in.-lb)
Low rotor	0.0347 (49.2%)	0.0139 (26.9%)	
High rotor	0.0207 (29.4%)	0.0130 (25.0%)	
Outer case	0.0144 (20.4%)	0.0051 (9.7%)	
Inner case	0.0007 (1.0%)	0 (0%)	
Springs		0.0199 (38.4%)	
Linear dampers			0.0882 (36.7%)
Viscous dampers			0.1522 (63.3%)

all critical speeds is apparent. The plot is similar to the filtered vibratory amplitude obtained during an engine test run in production or experimental test facilities.

Of particular importance to the design engineer is the kinetic and potential energy distribution at specific peak response speeds. These are shown in Table 1 and provide insight into the nature of the resonance so changes can be made to reduce the vibratory response, bearing loads, or rotor deflections. In addition, the three-dimensional mode shapes shown via two planes (Fig. 9) provide the relationship of the rotors and cases of the engine at specific response speeds. Collectively, this form of output provides the design engineer with sufficient analytical data to iterate upon the many variables within the engine to meet the design guidelines for an insensitive, lightweight engine.

Conclusions

It is essential to design aircraft powerplants with a rigorous dynamic response analysis. The entire engine structure must be analyzed in more detail than was originally thought possible to provide all engine critical speeds and response to imbalance. The knowledge of engine characteristics during the design and early development phases may prevent rotor dynamics problems that could seriously hinder development and service use. The two-plane multimass, multi-span forced response analysis presented herein is fully capable of predicting the response from imbalance of multi-shaft gas turbine engines. A unique transfer matrix method approach reduces the problem to only 16 simultaneous equations. The nonlinear damping elements (viscous dampers) commonly found in gas turbine engines to control vibration are incorporated directly into the analysis. This comprehensive analysis makes possible accurate steady-state response predictions of complex multi-shaft gas turbine engines.

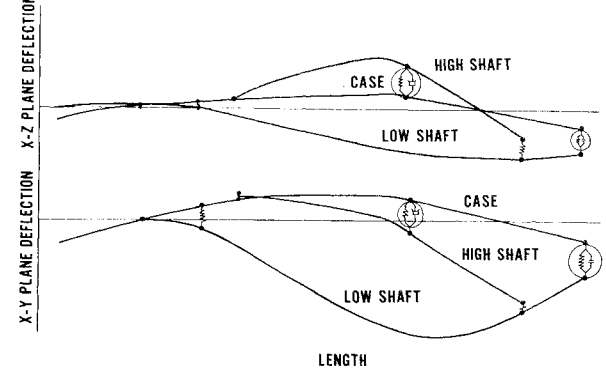

Fig. 9 Two-plane mode shape of two-shaft engine at 3200 rpm (low-rotor speed).

Appendix A: Transfer Matrix Influence Coefficient Analysis

The equations used to calculate the beam influence coefficients are derived in this Appendix. The general beam equations for a rotating shaft may be written as follows where the shaft properties are expressed per unit length.[8]

$$EI\frac{\partial^4 y}{\partial x^4} - \nu I\left(\frac{k_t E}{AG} + \frac{I_T}{\nu I}\right)\frac{\partial^4 y}{\partial x^2 \partial t^2} + \nu\frac{\partial^2 y}{\partial t^2} + \frac{k_t \nu I_T}{AG}\frac{\partial^4 y}{\partial t^4} - \omega I_p \frac{\partial^3 z}{\partial x^2 \partial t} + \frac{\omega \nu I_p k_t}{AG}\frac{\partial^3 z}{\partial t^3} = \omega^2 Uy + \frac{\omega^2 I_T k_t}{AG}\frac{\partial^2 Uy}{\partial t^2} + \frac{\omega^3 I_p k_t}{AG}\frac{\partial Uz}{\partial t} - \frac{\omega^2 EIk_t}{AG}\frac{\partial^2 Uy}{\partial x^2} \quad \text{(A1)}$$

$$EI\frac{\partial^4 z}{\partial x^4} - \nu I\left(\frac{k_t E}{AG} + \frac{I_T}{\nu I}\right)\frac{\partial^4 z}{\partial x^2 \partial t^2} + \nu\frac{\partial^2 y}{\partial t^2} + \frac{k_t \nu I_T}{AG}\frac{\partial^4 z}{\partial t^4} + \omega I_p \frac{\partial^3 y}{\partial x^2 \partial t} - \frac{\omega \nu I_p k_t}{AG}\frac{\partial^3 y}{\partial t^3} = \omega^2 Uz + \frac{\omega^2 k_t I_T}{AG}\frac{\partial^2 Uz}{\partial t^2} - \frac{\omega^3 I_p k_T}{AG}\frac{\partial Uy}{\partial t} - \frac{\omega^2 EIk_t}{AG}\frac{\partial^2 Uz}{\partial x^2} \quad \text{(A2)}$$

These equations are expressed in terms of the coordinate system shown in Fig. 10 for the x-y and x-z planes. The equations include the effect of rotary inertia, shear deformation, rotor spin effects, and an axial distribution of imbalance specified by (U_y, U_z). While it is possible to obtain solutions to these equations, it has been shown[8] that an approximate solution technique using lumped parameters can yield satisfactory results. Equations (A1) and (A2) may thus be significantly reduced by assuming the beam element to be massless. Hence, the beam equations reduce to Eq. (A3).

$$EI\frac{\partial^4 y}{\partial x^4} = 0 \qquad EI\frac{\partial^4 z}{\partial x^4} = 0 \quad \text{(A3)}$$

In terms of simple beam theory, including the effects of transverse shear deformation, the equation may be expressed as follows in x-y plane. Similar equations may be written for the x-z plane.

$$\frac{\partial}{\partial x}\left[EI\frac{\partial \theta}{\partial x}\right] + \frac{AG}{k_t}\left(\frac{\partial y}{\partial x} - \theta\right) = 0$$

$$\frac{\partial}{\partial x}\left[\frac{AG}{k_t}\left(\frac{\partial y}{\partial x} - \theta\right)\right] = 0 \quad \text{(A4)}$$

$$M = EI(\partial\theta/\partial x)$$

$$V = (AG/k_t)[\theta - (\partial y/\partial x)]$$

Referring to Fig. 10, the equation relating shear, moment, slope, and deflection at station n to the starred parameters at station n may be expressed considering Eq. (A4). These resulting transfer equations are as follows:

$$U_n = U_n^*$$

$$M_n = M_n^* + U_n l_n$$

$$\theta_n = \theta_n^* + \frac{l_n}{(EI)_n}M_n^* + \frac{l_n^2}{2(EI)_n}U_n^*$$

$$Y_n = Y_n^* + \theta_n^* l_n + \frac{l_n^2}{2(EI)_n}M_n^* + \left[\frac{l_n^3}{6(EI)_n} - \frac{k_t l_n}{(AG)_n}\right]V_n^* \quad \text{(A5)}$$

Similar expressions are valid for the x-z plane. The beam mass and gyroscopic properties are considered to be acting at the lumped mass station. The dynamic equations relating the shear and moment across the nth mass station are expressed in Eq. (A6).

$$U_n^* = U_{n-1} - m_n\frac{d^2 y_{n-1}}{dt^2} + u_n\omega^2\cos(\omega t + \phi_n)$$

$$V_n^* = V_{n-1} - m_n\frac{d^2 z_{n-1}}{dt^2} + u_n\omega^2\sin(\omega t + \phi_n)$$

$$M_n^* = M_{n-1} + I_T\frac{d^2\theta_{n-1}}{dt^2} + \omega I_p\frac{d\gamma_{n-1}}{dt} - T_n\omega^2\cos(\omega t + \eta_n) \quad \text{(A6)}$$

$$N_n^* = N_{n-1} + I_T\frac{d^2\gamma_{n-1}}{dt^2} - \omega I_p\frac{d\theta_{n-1}}{dt} + T_n\omega^2\sin(\omega t + \eta_n)$$

Considering circular synchronous motion at the frequency Ω, and introducing the notation $\beta_{Bn} = l_n/(EI)_n$, $\beta_{Sn} = k_t l_n/(AG)_n$, the equation relating the shear, moment, slope, and deflection at station $n + 1$ in the terms of their values at the nth station may be expressed by the following transfer equation:

$$\mathbf{U}_n = \mathbf{U}_{n-1} + m_n\Omega^2\mathbf{Y}_{n-1} + u_n\Omega^2\cos\phi_n$$

$$\mathbf{V}_n = \mathbf{V}_{n-1} + m_n\Omega^2\mathbf{Z}_{n-1} + u_n\Omega^2\sin\phi_n$$

$$\mathbf{M}_n = \mathbf{M}_{n-1} + \mathbf{U}_n l_n + \left[\frac{2\omega}{\Omega} - 1\right]\Omega^2 I_{g_n}\boldsymbol{\theta}_{n-1} - T_n\Omega^2\cos\eta_n$$

$$\mathbf{N}_n = \mathbf{N}_{n-1} + \mathbf{V}_n l_n + \left[\frac{2\omega}{\Omega} - 1\right]\Omega^2 I_{g_n}\boldsymbol{\Gamma}_{n-1} + T_n\Omega^2\sin\eta_n$$

$$\theta_n = \theta_{n-1} + \beta_{B_n}\left[\mathbf{M}_n - \frac{\mathbf{U}_n}{2}l_n\right] \quad \text{(A7)}$$

$$\boldsymbol{\Gamma}_n = \boldsymbol{\Gamma}_{n-1} + \beta_{B_n}\left[\mathbf{N}_n - \frac{\mathbf{V}_n}{2}l_n\right]$$

$$\mathbf{Y}_n = \mathbf{Y}_{n-1} + \theta_{n-1}l_n + \frac{\beta_{B_n}l_n}{G}[3\mathbf{M}_n - 2\mathbf{U}_n l_n] - \beta_{S_n}\mathbf{U}_n$$

$$\mathbf{Z}_n = \mathbf{Z}_{n-1} + \boldsymbol{\Gamma}_{n-1}l_n + \frac{\beta_{B_n}l_n}{G}[3\mathbf{N}_n - 2\mathbf{V}_n l_n] - \beta_{S_n}\mathbf{V}_n$$

These equations may be applied to each span to calculate the influence matrix α_{ij} and the column vector which expresses the influence of imbalance and moment loading along the span. They express the steady state response projection of the rotor system in the x-y and x-z planes at the reference time $\omega t = 0$. More elaborate beam elements may be considered by expressing the beam characteristics in terms of β_B and β_S.

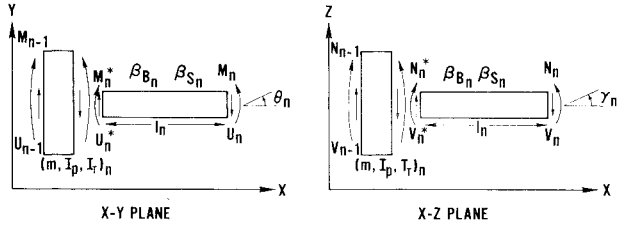

Fig. 10 Sign convention used in forced-response and critical-speed analyses.

Appendix B: Boundary Conditions and Compatibility Equations

The success of a dynamic-response analysis lies in the ease of operation for the design engineer. The description and formulation of the boundary conditions and compatibility equations for any equivalent engine system must be fully automated. To clarify these equations plus illustrate the unique line system influence coefficient approach, an example of a typical multi-line system follows.

For the two-line, multi-span system shown in Fig. 11, influence coefficients α_{ij} are calculated for each span as shown in Appendix A. In order to produce influence coef-

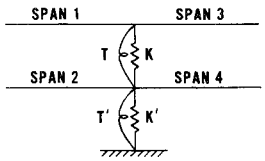

Fig. 11 Two-line system to illustrate influence coefficient calculation.

ficients, α_{ij}', across the entire line, transfer matrices at the junctions of spans are required. To transfer from the right side of span 1 to the left side of span 3, the four state variables at the right side of span 1 and 2 are assumed known. The matrix is constructed by standard boundary condition and compatibility equations in terms of the spring constants. Span 1 and span 3 transfer is shown in Eq. (B1).

$$\begin{bmatrix} \\ Q_3 \\ \\ \end{bmatrix}_{\text{LEFT}} = \begin{bmatrix} 1 & 0 & 0 & K & 0 & 0 & 0 & -K \\ 0 & 1 & T & 0 & 0 & 0 & -T & 0 \\ 0 & 0 & 1 & 0 & 0 & 0 & 0 & 0 \\ 0 & 0 & 0 & 1 & 0 & 0 & 0 & 0 \end{bmatrix} \begin{bmatrix} Q_1 \\ \\ \\ Q_2 \end{bmatrix}_{\text{RIGHT}}$$

$$= \begin{bmatrix} \\ R \\ \\ \end{bmatrix} \begin{bmatrix} Q_1 \\ \\ Q_2 \end{bmatrix} \tag{B1}$$

Similarly, the transfer from span 2 to span 4 is shown in Eq. (B2).

$$\begin{bmatrix} \\ Q_4 \\ \\ \end{bmatrix}_{\text{LEFT}} = \begin{bmatrix} 0 & 0 & 0 & -K & 1 & 0 & 0 & K' + K \\ 0 & 0 & -T & 0 & 0 & 1 & T + T' & 0 \\ 0 & 0 & 0 & 0 & 0 & 0 & 1 & 0 \\ 0 & 0 & 0 & 0 & 0 & 0 & 0 & 1 \end{bmatrix}$$

$$\times \begin{bmatrix} Q_1 \\ \\ \\ Q_2 \end{bmatrix}_{\text{RIGHT}} = \begin{bmatrix} \\ S \\ \\ \end{bmatrix} \begin{bmatrix} Q_1 \\ \\ \\ Q_4 \end{bmatrix}_{\text{RIGHT}} \tag{B2}$$

Since the influence coefficients, α_{ij}, for spans 1 and 2 are known, the variables at the right ends of spans 1 and 2 can be expressed in terms of the left end variables in a single matrix Eq. (B3).

$$\begin{bmatrix} Q_1 \\ Q_2 \end{bmatrix}_{\text{RIGHT}} = \left[\begin{array}{c|c} \alpha_{ij1} & 0 \\ \hline 0 & \alpha_{ij2} \end{array}\right] \begin{bmatrix} Q_1 \\ Q_2 \end{bmatrix}_{\text{LEFT}} \tag{B3}$$

By substituting Eq. (B3) into Eqs. (B1) and (B2), Eqs. (B4) and (B5) are obtained.

$$[Q_3]_{\text{LEFT}} = [R] \left[\begin{array}{c|c} \alpha_{ij1} & 0 \\ \hline 0 & \alpha_{ij2} \end{array}\right] \begin{bmatrix} Q_1 \\ Q_2 \end{bmatrix}_{\text{LEFT}} = [\alpha'_{ij1}] \begin{bmatrix} \Theta_1 \\ \gamma_1 \\ \Theta_2 \\ \gamma_2 \end{bmatrix}_{\substack{\text{LINE} \\ \text{LEFT}}} \tag{B4}$$

$$[Q_4]_{\text{LEFT}} = [S] \left[\begin{array}{c|c} \alpha_{ij1} & 0 \\ \hline 0 & \alpha_{ij2} \end{array}\right] \begin{bmatrix} Q_1 \\ Q_2 \end{bmatrix}_{\text{LEFT}} = [\alpha'_{ij2}] \begin{bmatrix} \Theta_1 \\ \gamma_1 \\ \\ \Theta_2 \\ \gamma_2 \end{bmatrix}_{\substack{\text{LINE} \\ \text{LEFT}}} \tag{B5}$$

Since the variables V and M at the left side of all lines are either zero or defined in terms of slope and deflection, the four variables at the left of spans 3 and 4 can be written in terms of slope and deflection via the α_{ij}' matrix. This approach is continued across all lines, through each span until ultimately the variables at the right side of each line are expressed in terms of the slope and deflection at the left ends of all lines. Thus, a compact and small matrix A_{ij}, Eq. (5), is generated to provide critical speeds and forced response for a multi-shaft gas turbine engine.

Appendix C: Energy Equations

The kinetic energy of each inertial mass is defined by Eq. (C1).

$$KE = \frac{1}{2} \frac{m\Omega^2}{g} (\mathrm{Y}^2 + \mathrm{Z}^2) + \frac{I_g \omega^2}{g} - \frac{I_g \Omega}{2g} (2\omega - \Omega)(\Theta^2 + \Gamma^2) \tag{C1}$$

The bending and shear strain energies within each beam element are defined in Eqs. (C2) and (C3).

$$SE_{\text{BEND}} = (l/6EI)(\mathrm{M}^{*2} + \mathrm{M}^*\mathrm{M} + \mathrm{M}^2 + \mathrm{N}^{*2} + \mathrm{N}^*\mathrm{N} + \mathrm{N}^2) \tag{C2}$$

$$SE_{SHEAR} = (K_t l/2AG)(\mathrm{U}^2 + \mathrm{V}^2) \tag{C3}$$

The strain energy in the radial and torsional springs is defined in Eq. (C4).

$$SE = (1/2)[K(\mathrm{Y}^2 + \mathrm{Z}^2) + T(\Theta^2 + \Gamma^2)] \tag{C4}$$

The energy dissipated per cycle by a damper is shown in Eq. (C5).

$$E_D = 2\pi\Omega B(\mathrm{Y}^2 + \mathrm{Z}^2) \tag{C5}$$

Appendix D: Viscous Damper Stiffness and Damping Analysis

The viscous damper analysis used in conjunction with the linear forced response analysis is a modification of the original Sommerfeld solution of the plain journal bearing by Pinkus and Sternlicht.[12] This original work by Sommerfeld consisted of solving the Reynolds equation for the case of fluid within circular cylinders of infinite length (no end leakage) and a complete 2π film. The 2π film can be shown analytically to have no radial restoring force and hence no stable steady-state solution. Pinkus and Sternlicht's modification forces the pressure and pressure gradient to zero at some angle θ. All negative pressures are set to zero. The Reynolds equation, Eq. (D1), relates the circumferential pressure profile and the spin and whirl velocity within infinitely long cylinders.

$$\frac{1}{6R^2} \frac{\partial}{\partial\Theta} \left(\frac{h^3}{\mu} \frac{\partial P}{\partial\Theta} \right) = (\omega_1 + \omega_2 - 2\Omega) \frac{\partial h}{\partial\Theta} + 2 \frac{\partial h}{\partial t} \tag{D1}$$

For a viscous damper with nonrotating inner and outer cylinders and circular whirl is the only form of motion: i.e., $\omega_1 = \omega_2 = 0$ and $\partial h/\partial t = 0$, Eq. (D1) reduces to Eq. (D2).

$$\frac{\partial}{\partial\theta} \left(\frac{h^3}{\mu} \frac{\partial P}{\partial\theta} \right) = -12R^2\Omega \frac{\partial h}{\partial\theta} \tag{D2}$$

This differential equation is a particular form of the Reynolds equation directly applicable to the viscous damper. It relates the pressure distribution within the damper to the whirl speed. The step-by-step detailed solution to this equation is developed in Ref. 12. The final solution with the boundary conditions [Eq. (D3)] applied is shown in Eq. (D4).

$$\begin{gathered} P = 0 \;@\; \theta = 0 \\ dP/d\theta = 0 \;@\; \theta = \theta_0 \\ P = 0 \;@\; \theta = \theta_0 \end{gathered} \tag{D3}$$

$$P = \frac{12\mu R^2\Omega}{C^2(1 - \epsilon^2)^{3/2}} \left\{ \psi - \epsilon \sin\psi - \frac{(2 + \epsilon^2)\psi - 4\epsilon \sin\psi + \epsilon^2 \sin\psi \cos\psi}{2(1 - \epsilon \cos\psi_0)} \right\} \tag{D4}$$

where

$$\cos\psi = [(\epsilon + \cos\theta)/(1 + \epsilon\cos\theta)]$$

ψ_0 corresponds to θ_0 and is related to ϵ by Eq. (D5).

$$\epsilon(\sin\psi_0' \cos\psi_0' - \psi_0) + 2(\psi_0 \cos\psi_0' - \sin\psi_0') = 0 \tag{D5}$$

where

$$\psi_0' = \psi_0 - \pi$$

The stiffness (K) and damping (B) coefficients are defined as the forces opposing the components of the pressures load W, i.e.,

$$Ke = W\cos\phi = \int_0^{2\pi} LRP\cos\theta d\theta$$
$$Be\Omega = W\sin\phi = \int_0^{2\pi} LRP\sin\theta d\theta \tag{D6}$$

Upon substituting for P and integrating in terms of the variable ψ from 0 to ψ_0, Eq. (D7) and (D8) are obtained.

$$W\cos\theta = \frac{-6\mu R\Omega L\epsilon\left(\frac{R}{C}\right)^2(1 + \cos\psi_0')^2}{(1 - \epsilon^2)(1 + \epsilon\cos\psi_0')} \tag{D7}$$

$$W\sin\theta = \frac{12\mu R\Omega L\left(\frac{R}{C}\right)^2(\psi_0\cos\psi_0' - \sin\psi_0')}{(1 - \epsilon^2)^{1/2}(1 + \epsilon\cos\psi_0')}$$

$$W = \frac{6\mu R\Omega L(R/C)^2}{(1 - \epsilon^2)^{1/2}(1 + \epsilon\cos\psi_0')}\left[\frac{\epsilon^2(1 + \cos\psi_0')^4}{1 - \epsilon^2} + 4(\psi_0\cos\psi_0' - \sin\psi_0')^2\right] \tag{D8}$$

$$\tan\phi = \frac{-2(1 - \epsilon^2)^{1/2}(\sin\psi_0' - \psi_0\cos\psi_0')}{\epsilon(1 + \cos\psi_0')^2}$$

The Sommerfeld number S is defined in terms of load P in Eq. (D9) and (D10).

$$S = \frac{\mu N}{P}\left(\frac{R}{C}\right)^2 \tag{D9}$$

$$P = \frac{W}{LD} \text{ and } N = \frac{\Omega}{2\pi} \tag{D10}$$

Upon substituting Eq. (D10) into Eq. (D9), a viscous damper Sommerfeld number is defined [Eq. (D11)] for a specific damper load W.

$$S_{VD} = \frac{\mu\Omega LD^3}{8\pi WC^2} \tag{D11}$$

By solving Eq. (D11) for the damper load W and substituting into Eq. (D6) the component damper forces are obtained [Eq. (D12)].

$$K = \frac{\mu\Omega LD^3}{8\pi S_{VD}\epsilon C^3}\cos\phi \tag{D12}$$
$$B = \frac{\mu LD^3}{8\pi S_{VD}\epsilon C^3}\sin\phi$$

References

[1]Myklestad, N. O., "A New Method of Calculating Natural Modes of Uncoupled Bending Vibration of Airplane Wings and Other Types of Beams," *Journal of Aeronautical Sciences*, Vol. 11, April 1944, pp. 153–162.

[2]Prohl, M. A., "A General Method for Calculating Critical Speeds of Flexible Rotors," *Journal of Applied Mechanics*, Sept. 1945, pp. 142–148.

[3]Green, R. B., "Gyroscopic Effects on the Critical Speeds of Flexible Rotors," *Journal of Applied Mechanics*, Dec. 1948, pp. 369–376.

[4]Yamamoto, T., "On the Critical Speeds of a Shaft," *Memoirs of the Faculty of Engineering*, Nagoya University, Japan, Vol. 6, Nov. 1954, pp. 106–174.

[5]Koenig, E. C., "Analysis for Calculating Lateral Vibration Characteristics of Rotating Systems With Any Number of Flexible Supports; Part 1, Method of Analysis," *ASME Transactions, Journal of Applied Mechanics*, Vol. 28, 1961, pp. 585–590.

[6]Tang, T. M. and P. R. Trumpler, "Dynamics of Synchronous Precessing Turbo-Rotors with Particular Reference to Balancing; Part 1, Theoretical Foundations," *ASME Transactions, Journal of Applied Mechanics*, Vol. 31, March 1964, p. 115.

[7]Lund, J. W., "Rotor-Bearing Dynamics Design Technology, Part V," Technical Report AFAPL-TR-65-45, Aero Propulsion Lab, Wright-Patterson Air Force Base, Dayton, Ohio, May 1965.

[8]Lund, J. W. and F. K. Orcutt, "Calculations and Experiments on the Unbalance Response of a Flexible Rotor," *ASME Transactions Journal of Engineering for Industry*, Series B, Vol. 89, Nov. 1967, pp. 785–796.

[9]Lemke, D. G. and Trumpler, R. P., "On Dynamic Response of Axially Coupled Turborotors," *ASME Transactions, Journal of Engineering for Industry*, Vol. 94, No. 2, May, 1972.

[10]Sevcik, J. K., "System Vibration and Static Analysis," ASME Paper 63-AHGT-57, Gas Turbine Conf., Los Angeles, Calif., March 1963.

[11]Bohm, R. T., "Tame the Menace of Turbine Vibration," *SAE Journal*, Feb. 1966, pp. 44–48.

[12]Pinkus, O. and Sternlicht, B., *Theory of Hydrodynamic Lubrication*, McGraw-Hill, New York, 1961.